

# Phenomenology of pulsar B0809+74's rotating subbeam system

## II. “Carousel” configuration and polarization

Joanna M. Rankin<sup>1,\*</sup>, R. Ramachandran<sup>2</sup>, Joeri van Leeuwen<sup>3</sup>, and Svetlana A. Suleymanova<sup>4,5</sup>

<sup>1</sup> Sterrenkundig Instituut “Anton Pannekoek”, 1098 SJ Amsterdam, The Netherlands  
e-mail: jrankin@astro.uva.nl; joanna.rankin@uvm.edu

<sup>2</sup> Department of Astronomy, University of California, Berkeley, CA 94720, USA  
e-mail: ramach12@gmail.com

<sup>3</sup> Department of Physics & Astronomy, University of British Columbia, Vancouver, V6T 1Z1 Canada  
e-mail: joeri@astro.ubc.ca

<sup>4</sup> Pushchino Radio Astronomy Observatory, 142290 Pushchino, Russia  
e-mail: suley@prao.psn.ru

<sup>5</sup> Isaac Newton Institute of Chile, Pushchino Branch

Received 26 October 2005 / Accepted 6 January 2005

### ABSTRACT

Building on results and analyses of previous works, the structure and polarization of B0809+74's subbeam “carousel” is delimited, but not fully solved. Some 8–10 subbeams are indicated for an equatorward sightline traverse and 25–40 for a polarward one. Either alternative indicates a subbeam circulation time much longer than predicted by theory. Polarized subbeam maps show complex structure and suggest that the star's polarized modes are angularly disjoint.

**Key words.** stars: pulsars: individual: B0809+74 – polarization – radiation mechanisms: non-thermal

### 1. Introduction

Pulsar B0809+74 provides one of the richest contexts for studying pulsar emission physics. As noted in the foregoing paper (Rankin et al. 2006, hereafter Paper I), it exhibits all six of the heretofore well identified phenomena: subpulse drifting, pulse nulling, profile mode switching, polarization modes, microstructure, and profile “absorption”.

B0809+74's much studied ~11-period fluctuation feature was first noticed by Taylor et al. (1969), only a few months after Drake & Craft's (1968) early identification of “drifting” subpulses (in B1919+21 & 2016+28), but their poor resolution caused them to doubt its significance. Vitkevich & Shitov, in January 1970, then first exhibited the star's 11-period subpulse drift using (November 1968) Pushchino Observatory observations at 86 MHz with adequate sensitivity and time resolution. One month later, Sutton et al. confirmed the precisely drifting pulse sequences (hereafter PSs) using Green Bank data, and also introduced the now standard terminology of  $P_1$ ,  $P_2$  and  $P_3$  for the pulsar rotation period, the subpulse-separation interval, and the driftband-separation period, respectively. Cole (1970) then first showed that the subpulse-drift rate was occasionally irregular. Taylor & Huguenin (1971) first demonstrated the star's remarkably stable 11- $P_1$  modulation feature via a fluctuation spectrum, while also showing that it occasionally “ceased pulsing” for a few periods. The phenomenology and interpretation of such “drifting” was systematized and quantified by

Backer (1970a–d, 1971, 1973), who also discovered the “nulling” effect, through introduction of both longitude-resolved fluctuation (hereafter LRF) spectra and fluctuation-phase diagrams – although these methods were not applied to B0809+74 until later (Backer et al. 1975). Furthermore, impressed by these early observations, Ruderman (1972) first associated such “drifting” subpulses with a system of subbeams circulating under the action of  $\mathbf{E} \times \mathbf{B}$  drift (see also Ruderman & Sutherland 1975; and Ruderman 1976).

The discovery by Page (1973) first that the “drift” rate is suppressed just after a null and second that the subpulse phase remains nearly stationary across a null gave rise to the dilemma of subpulse “memory”, a jargon for the unknown physical processes which restart a subpulse at very nearly the same position where it had disappeared. The paper also introduced the method of following the driftband phase over many successive bands, and showed that the drift rate exhibits perplexing variations with longitude, at different frequencies, and (more subtly) at different epochs. Five further papers attempted to refine and explain this remarkable phenomenon. Unwin et al. (1978) used a drift-band filter technique to exhibit the post-null recovery behavior so clearly that it inspired further analyses (Popov & Smirnova 1982; Filippenko et al. 1983) and a thoughtful attempt to understand the “memory” within the context of existing theory (Filippenko & Radhakrishnan 1982). Finally, Lyne & Ashworth's (1983) comprehensive (and ostensibly independent) work showing an apparent exponential post-null drift-rate recovery has widely been quoted as the definitive analytical description of the “memory” phenomenon.

\* On leave from Physics Dept., University of Vermont, Burlington, VT 05405 USA.

In the course of a recent reexamination of the drift and null phenomena exhibited by B0809+74, van Leeuwen et al. (2002) have shown that the above exponential decay is only apparent in the average behavior; the individual post-null drift-speed changes are usually much more rapid. Also, the star exhibits several unusual but distinct modulation “states” at meter wavelengths, which produce profile mode-changing effects similar to those seen in many other pulsars. As with the “B” and “Q” modes of B0943+10 (Deshpande & Rankin 1999, 2001; hereafter DR99 and DR01), the modal profiles exhibit varying levels of asymmetry in the emission (or “absorption”) about the longitude of the magnetic axis. They develop techniques whereby most of the pulsar’s nulls can be reliably identified, assess how nulls affect the drift, and show that null removal restores drift-band continuity and periodicity to first order. Van Leeuwen et al. (2003) are then able to demonstrate, using these methods, that the star’s 11- $P_1$  fundamental drift modulation cannot be aliased – a result of primary significance in our further analyses below.

The role of the polarization modes was not fully studied in B0809+74 until recently, because the early polarimetric studies of this pulsar (Taylor et al. 1971; Lyne et al. 1971) were carried out before this phenomenon was well identified (Manchester et al. 1975; Backer & Rankin 1980). Ramachandran et al. (2002) have demonstrated their determinative role in the star’s PS polarization, and it is now clear that the star’s largely complete profile depolarization at meter wavelengths is typical of the ( $S_d$ ) pulsar class (Rankin & Ramachandran 2003) where the sightline runs tangentially along the outside conal edge. Both the linear depolarization and slightly nonorthogonal polarization-mode mixing in this outside conal edge region of the emission beam tend to distort the overall average polarization-angle (hereafter PA) traverse and frustrate any ready geometrical interpretation for such stars (e.g., Lyne & Manchester 1988; Rankin 1993a,b). It has been possible to show that the complex polarization-modal structure of the drifting subpulses in B0809+74 are largely responsible for the old and perplexing reports of both longitude and frequency variations in the subpulse interval  $P_2$  (Rankin et al. 2005, hereafter RRS; see also Edwards & Stappers 2003, 2004).

Paper I further provides a careful determination both of the star’s PA sweep rate and of its profile evolution as complicated by “absorption”. The PA ( $\chi$ ) rate  $R (= \Delta\chi/\Delta\varphi)$  with longitude ( $\varphi$ ) was found to be  $-1.83 \pm 0.11$ . These factors are used to construct an overall model of its emission geometry<sup>1</sup>, including the extent of its profile “absorption”, and we will make considerable use of this analysis in what follows.

In this paper, we will now apply to B0809+74 the techniques developed by Deshpande & Rankin (1999, 2001) for B0943+10. We have learned, in the course of the challenging analyses outlined above, that B0943+10 is in many respects a simpler star. It apparently does not null. Its modes persist for many thousands of pulses. Its PSs are usually dominated by one polarization mode, and no microstructure has been identified in its subpulses. Paper I Sect. 2 describes the observations on which our analyses here are based. In Sect. 2 of this paper we undertake a basic fluctuation-spectral analysis of the star’s PSs. Section 3 recounts our efforts to determine the star’s subbeam-“carousel” circulation time, Sect. 4 describes how the polarized subbeam structure is mapped, and in Sect. 5 we summarize and discuss the results.

<sup>1</sup> The star’s magnetic latitude  $\alpha$  and sightline impact angle  $|\beta|$  were found to be some 8.5–9.0 and 4.5–4.9°, respectively, using the fact that  $R = \sin \alpha / \sin \beta$ .

## 2. Subpulse modulation and polarization

Unlike pulsar B0943+10, B0809+74 exhibits occasional “null” pulses, and we noted above that these have been the subject of considerable study, because the subpulse drift appears to halt, at least approximately, during null intervals. For the exceptionally bright 328-MHz WSRT observation of 2000 November 26<sup>2</sup> and certain others, it has been possible to identify these nulls quite positively, because the intensity distributions of the non-null and null pulses are disjoint (see van Leeuwen et al. 2002: Fig. 1). Most of the star’s nulls are brief (1–3 pulses), but nulls as long as some 15 pulses have been observed (see above: Fig. 4)<sup>3</sup>. Indeed, closer study shows that there is a small phase jump associated with each null (above: Fig. 5); however this mean step is so small (typically some 20% of  $P_2$ , the interval between adjacent subpulses) that it can be ignored. Several historical studies (Unwin et al. 1978; Lyne & Ashworth 1983) have also shown that the coherence of the pulsar’s drifting pattern is enhanced by removing the nulls (see their Figs. 8 and 12, respectively), so we have followed this procedure.

Figures 1a and b give longitude- and harmonic-resolved (hereafter LRF and HRF) fluctuation spectra for pulsar B0809+74 at 328 MHz, using the bright 2000-November-26 PS mentioned above. The analytical methods used in computing these spectra are identical to those in Deshpande & Rankin (2001), except that here we have used PSs in which the null pulses have been removed. In the relevant section of the PS, there are several short nulls, and though we have reliably identified them using the methods of van Leeuwen et al. and constructed a “null removed” PS – shortened by the number of null pulses encountered and thus providing a first-order correction for the drift-phase hiatus the nulls produce – we still see a somewhat diminished  $Q$  factor (=frequency/half power width) in the primary modulation feature as compared with (unfortunately weaker) intervals of the sequence which are free of nulls. Here we have used FFTs of length 512 (LRF) and 256 (HRF) to study the total-power (Stokes  $I$ ) sequence, and Fig. 1 demonstrates clearly how strongly and fully the star’s “drifting” subpulses modulate its PSs.

Several other aspects of Fig. 1a also deserve mention. First note the pulsar’s 328-MHz average Stokes  $I$  profile in the left-hand panel and that we have taken the zero-point of longitude, corresponding to that of the magnetic axis, well on its leading edge – a determination guided by the “absorption” model in Paper I, Table 2. The LRF spectra are plotted in the central panel as contours and the strong feature corresponding to the 10.89- $P_1$  primary modulation is very prominently in evidence. The bottom panel then represents the longitude integral of the spectral power, and here the narrowness (high  $Q$  factor) of the modulation feature is most clear. Indeed, the feature is barely resolved, and its low level structure is of uncertain significance. Note also that the spectrum is so “clean” that the feature’s first harmonic at some 0.184 cycles/ $P_1$  (hereafter  $c/P_1$ ) can be discerned – and, in other sections of our observations it is often even more prominent.

The HRF spectrum in Fig. 1b is no less interesting. Here we have used eight contour levels to cover the lowest 5% of the amplitude of the primary feature in the central panel in order to emphasize the structure of the spectrum just above the noise

<sup>2</sup> The resolution of this and other WSRT observations is 0.114°, here following from use of 256 channels across a 10-MHz bandwidth.

<sup>3</sup> The foregoing paper further implies that there is a population of unobservable nulls lasting for less than one period which can of course not readily be detected and removed.

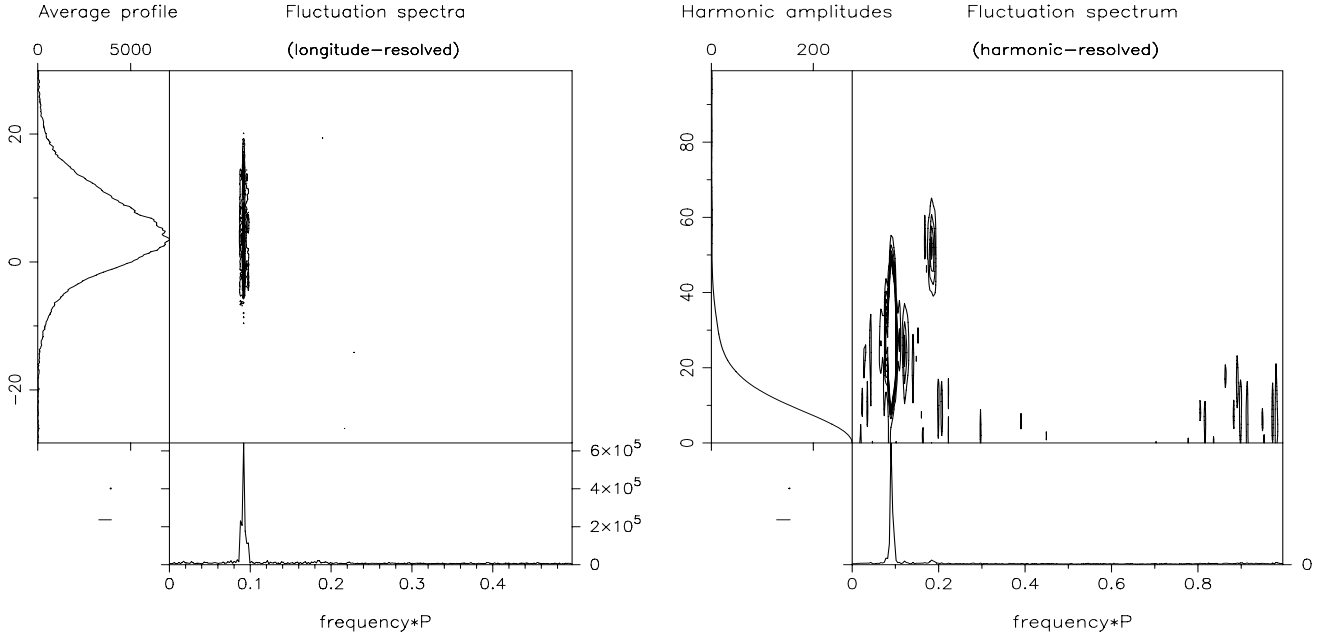


**Fig. 1.** Longitude-resolved (a, left) and harmonic-resolved (b, right) fluctuation spectra for pulsar B0809+74 at 328 MHz, computed using a WSRT PS recorded on 2000 November 26. The analysis was applied to the total power (Stokes  $I$ ) and used FFTs of length 512 and 256, respectively. The three panels of the left-hand LRF display give the pulsar’s average profile (left), LRF spectra (centre), and integral spectrum, (bottom) respectively; whereas, those of the right-hand HRF display give the (integer) harmonic amplitudes of the average profile (left), the non-integer harmonic amplitudes associated with the modulation (centre), and the integral fluctuation spectrum (bottom). See DR01 for a complete description. The central panels of both displays use 8 contour levels; however, these cover only the lowest 5% of the feature amplitude of the HRF spectrum in order to exhibit the lowest level features. Note also that the longitude origin of the average profiles has been taken just above the half-power point on the profile’s leading edge, following the analysis of Paper I.

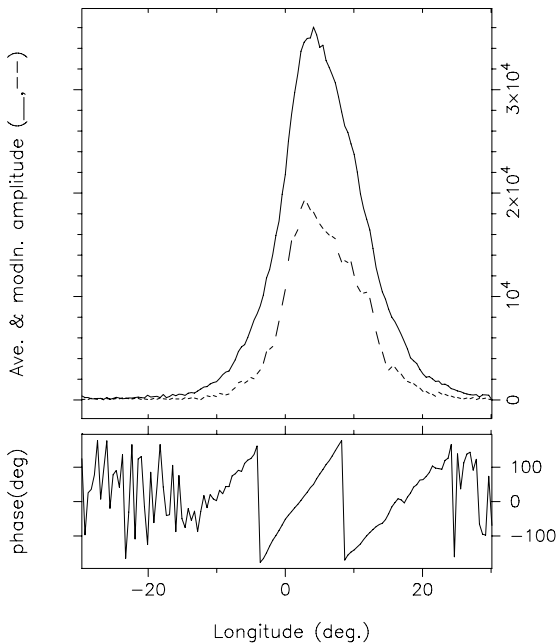


**Fig. 2.** Fluctuation-spectral phase and modulation amplitude at 328 MHz corresponding to the primary  $0.092 c/P_1$  feature in Figs. 1a and b. Fluctuation power is plotted as a function of longitude within the average profile in the top panel, whereas the fluctuation phase is given in the lower panel.

level. Thus we see the broadened pattern corresponding to the primary feature, whose maximum falls at harmonic numbers in the 25–30 range. The first harmonic appears more clearly here with peak harmonics at about 50–55. Note that little else can be said: overall, the panel is conspicuously blank, and the few

other responses appear to represent either noise fluctuations or exceedingly weak periodicities of uncertain significance.

Figure 2 again gives the 328-MHz average profile, but here we plot the relative amplitude of the primary modulation (corresponding to the peak frequency in Fig. 1 only) as well as its phase behavior as a function of pulse longitude. Here we again see evidence of the remarkable complexity behind the star’s highly orderly subpulse “drift”: the phase rate is not entirely linear but varies across the pulse profile, being greatest near the longitude origin as expected. The modulation-phase gradient (in units of cycles/°) is the inverse of the subpulse spacing  $P_2$ , so its variation can be interpreted as a longitude dependence of  $P_2$ . The variation is surely not entirely geometric, however. As noted above, many early studies report drift-rate, subpulse-width and  $P_2$  changes as a function of longitude, radio frequency and epoch – but it is important to recall that all of these studies (and this one here) analyzed only the total power, Stokes parameter  $I$ . These apparent  $P_2$  variations are exhibited very clearly in Fig. 3 of van Leeuwen et al. (2002) as residuals to linear fits to the drift-band position and slope.

Indeed, the pulsar’s  $P_2$  variation has now received considerable recent study. Edwards & Stappers (2003) have drawn attention to anomalies in the subpulse drift of both B0320+39 and B0809+74, arguing that drift-modulation systems with phase offsets can both curve driftbands and produce phase discontinuities, such as those seen in the pulsar at 21 cms. More specifically, Rankin & Ramachandran (2003) and RRS show that two offset systems of modal “beamlets” are encountered along the sightline traverse, and these produce complex modal polarization effects that appear as  $P_2$  variations in total power. The latter paper’s Fig. 2 surely demonstrates how complex and frequency sensitive these effects are, particularly at higher frequencies.

Overall, the driftbands are relatively linear at 100 MHz and below, show very discernible curvature at 300 MHz as we see here, and above 1 GHz produce puzzling discontinuities in the phase rate of the drift modulation.

We can thus be confident that modal polarization plays a major role in the observed  $P_2$  anomalies, but we do not yet know what characteristics of modal subbeam structure give rise to them. We will therefore return to these issues below and in subsequent studies.

### 3. Efforts to determine B0809+74' subbeam configuration and circulation time

A major objective, of course, in our work on pulsar B0809+74 has been to determine its subbeam configuration and circulation time. When this effort began, the DR99 and DR01 work on pulsar B0943+10 was very present in our minds, and we expected to find, very likely with some difficulty, signatures in its fluctuation spectra comparable to those in the latter pulsar, which would guide us in determining its subbeam circulation characteristics. We also then considered – extrapolating from B0943+10's properties using the Ruderman & Sutherland (1975) theory – that its circulation time might be as short as  $6.4 P_1$  and thus likely highly aliased. Finally, we expected to use the inverse-cartographic transform search technique described in DR01 to confirm the circulation time and geometrical parameters.

Wrong – and it is perhaps useful to summarize the course of this failed “0943ish” strategy which was pursued in numerous forms and variations over several years time. As we mentioned above in the course of discussing Figs. 1 and 2, one sees very little in this star's fluctuation spectra, apart from the narrow primary modulation feature and its first harmonic. Multiple null-removed sequences were searched, as well as a lengthy 355-MHz WSRT sequence which is free of observable nulls for a remarkable 858 pulses! These efforts provided no information apart from  $P_3$  through fluctuation-spectral analyses.

Extensive efforts were then made to use the inverse-cartographic transform method, not to confirm the circulation properties, but to determine them. This work entailed measuring  $P_3$  accurately for a given high quality PS and then testing all combinations of alias order, subbeam number, drift direction, inner/outer sightline traverses, and often  $R$  values<sup>4</sup> over a specified range to see which matched best with the observed sequence. Recall that this method constructs a polar emission map from the observed PS using the specified parameters, generates an artificial PS from this trial polar map, and then correlates the artificial PS with the observed one in order to determine which set of parameter values best reproduces the natural PS.

Multiple full searches were computed for a variety of promising PSs at different frequencies for alias orders between zero and 6, subbeam numbers between 3 and 32, poleward and equatorward sightline traverses, and all combinations of stellar and subbeam carousel rotation direction. No specific configuration was identified as had been for B0943+10. In general, the efforts showed a) that 13–17 beams were indicated for a poleward sightline traverse and 6–8 for an equatorward one, irrespective of the alias order, and b) the correlations were always

highest for alias order zero (i.e., no aliasing) and declined steadily for higher alias orders. The subbeam configurations were thus just what could be expected geometrically, without aliasing (e.g., per the model in Table 2 of Paper I as computed using the steeper  $R$  value then thought to obtain). Without aliasing, however, the circulation time  $\hat{P}_3$  is just the product of  $P_3$  and the subbeam number  $N$  – some 130–170  $P_1$  – values which initially seemed so long that they could not possibly be correct<sup>5</sup>.

The null-analysis studies of van Leeuwen et al. (2002, 2003) then provided a new line of evidence that B0809+74's circulation time is indeed very long. The arguments in the second paper – to the effect that we could not fail to observe the effects of aliasing (if it existed) as the subbeam carousel accelerates following a long null – now seem to us definitive. And, this corroborates our early experience with the inverse-cartographic searches, in which the largest correlations always result for alias order 0. The aliasing then apparently settled, the “carousel” circulation time  $\hat{P}_3$  will be  $N$  times  $P_3$  ( $=11P_1$ ) – an interval which will be longer or much longer than that of B0943+10 (contrary to R&S) for any reasonable geometrical estimate of the subbeam number  $N$ .

We have now carried out a new series of inverse-cartographic searches which reflect our understanding that a) the subpulse modulation in B0809+74 is not aliased, and b)  $R$  is some  $-1.83$ . None of these analyses results in a single preferred value of  $N$ , but they do restrict the range of  $N$  to some 8–12 if  $\beta > 0$  (outside, equatorward sightline traverse) and in the 25–40 range if  $\beta < 0$  (inside, polarward traverse). We have carried out searches on the 112.7, 328, 355, and 1380-MHz observations described in Paper I Table 1, using the geometrical models in its Table 2 as well as computing direct autocorrelation functions for each sequence which require no such model. The searches explored  $N$  values up to 60, and the direct autocorrelations up to delays of 511 pulses, giving an effective maximum  $N$  of almost 47. Two different indicators were used for assessing the quality of the inverse-cartographic transform, the direct zero-delay cross-correlation (hereafter CCF) value between the natural and artificial PSs and their modulation-phase difference.

Overall, the correlations provided little specificity. The  $\beta < 0$  CCFs tended to show a broad decrease in the correlation (both direct and in terms of the inverse-cartographic beam maps) which had minima in the 15–25 range, and broad maxima for  $N$  values of 25–40. The modulation-phase measure in some cases exhibited a fairly sharp minimum in the same 25–40 range, but no consistent value of  $N$  was indicated. Almost exactly the same kind of result was obtained for the  $\beta > 0$  searches. All showed broad maxima (minima for the phase) in the 8–12 range, and those with the best defined minima (the 328- and 113-MHz observations) pointed to  $N$  values of 8 and 11, respectively.

For the inverse-cartographic searches it is difficult to assess just how much the maxima merely reflect the particulars of the geometrical model of Table 2. However, most of the direct autocorrelations – carried out on our null-removed PSs – exhibit the same broad maxima out to a lag of perhaps 100 and then in the range around 300–500 pulses, which correspond again to  $N$ s in the ranges above. We have also experimented with correlations of the linearly polarized power alone, using the artificial Stokes parameter  $Q'$  rotated so as to represent almost all of the polarized power – and these tend to give weaker but

<sup>4</sup> A major overall problem with these early searches was that  $R$  then was thought to be near  $-2.75$  as indeed can be inferred from Ramachandran et al.'s (2002) Fig. 1; only after the recent WSRT polarimetry recalibration (Edward & Stappers 2004) could it be understood that most of Stokes  $V$  was uncorrected  $Q$  or  $U$ , with the ultimate result that  $R$  is nearly a crucial full unit less steep as we have computed in Paper I Sect. 3.

<sup>5</sup> Another difficulty with this early work was an incorrect tendency to believe that the star had a poleward (or inside) sightline geometry, based on the “rule” just below Eq. (4) in DR01. This line of argument is only relevant when the subbeam number  $N$ , and thus the magnetic azimuth angle between subbeams  $\eta$  ( $=360^\circ/N$ ), is known independently.

comparable indications, perhaps simply due to the attenuated signal power compared to the noise level.

In any case, it is not clear how strong a correlation signature could be expected at the possible 100–400-odd pulse or 1–5 min interval corresponding to B0809+74’s circulation time. Even in very unusual circumstances such as the 858-pulse null-free PSs mentioned above, presumably the individual subbeam intensities will become decorrelated. In B0943+10 observations seemed to show that the circulating subbeams retained some correlation only for perhaps 100 s, and surely not in all PSs even for this long. We have thus made every attempt to determine a definite and exact circulation time for B0809+74 and failed, so we do not know how such a determination might be made in future. However, our overall analysis efforts have had the effect of showing approximately what B0809+74’s subbeam configuration and circulation time must be – and again it most probably entails either an outer sightline traverse with some 9–11 subbeams and a  $\dot{P}_3$  value between 75 and 90 secs or and inner traverse with 25–40 subbeams and a  $\dot{P}_3$  of between 6 and 9.5 min.

Finally, notice that we have computed  $P_2$  values in the rightmost column of Paper I’s Table 2. These are computed by dividing magnetic azimuth into an appropriate number of equal intervals corresponding to the estimated number of subbeams, and then using the geometrical relationship in DR01: Eq. (3) to calculate the longitude separation between a pair of subbeams centered on the magnetic-axis longitude. For this computation, and for an outer sightline traverse, we have found that an  $N$  of 10 most accurately agrees with the available  $P_2$  values in the literature, which are also summarized in RRS. For an inner traverse (not shown) an  $N$  of 34 was found to result in  $P_2$  values that were identical to those shown within a tenth of a degree. Notice that in terms of this geometric model,  $P_2$  is nearly constant at 100 MHz and above; only at very low frequencies does it exhibit a significant increase.

We end this section by returning to the 40.1-MHz correlation plot in Paper I: Fig. 5. Note that sections of five linear drift bands can be discerned, and the interval between adjacent bands, measured parallel to the axes is about 15–17°, thus agreeing decently with the model  $P_2$  value in the paper’s Table 2.

#### 4. Mapping the polarized subbeam structure

Let us now examine pulsar B0809+74’s “carousel”-beam structure, knowing now from Paper I and the above discussions something of the star’s basic emission geometry, the longitude position of the magnetic axis (e.g., as depicted in Fig. 3 based on the models of Paper I, Table 2), and a resolution of the complex  $P_2$  issues which were the subject of RRS. We can view the subbeam system as a steadily rotating “carousel” with a fairly definite subbeam configuration and thus circulation time in each of two possible geometrical circumstances: an “inner” or “outer” sightline traverse.

Figure 3 gives a 34-beam total-power subbeam map, corresponding to an “inner” or poleward sightline traverse, for the 328-MHz observation in Fig. 1. This is just the configuration obtained for B0943+10, but there the smaller  $P_3$  and steeper  $R$  indicated an  $N$  of about 20 (which was then confirmed by fluctuation-spectral analysis). While we cannot now know whether this is the correct “carousel” configuration, in practical terms the large number of “beamlets” makes it difficult to see the individual beamlet characteristics. We will thus concentrate below on the “outer”, positive- $\beta$  geometry where about 10 subbeams are indicated.

To explore the subbeam polarization behavior, we have mapped the beamlet structure in linear polarization as well as in

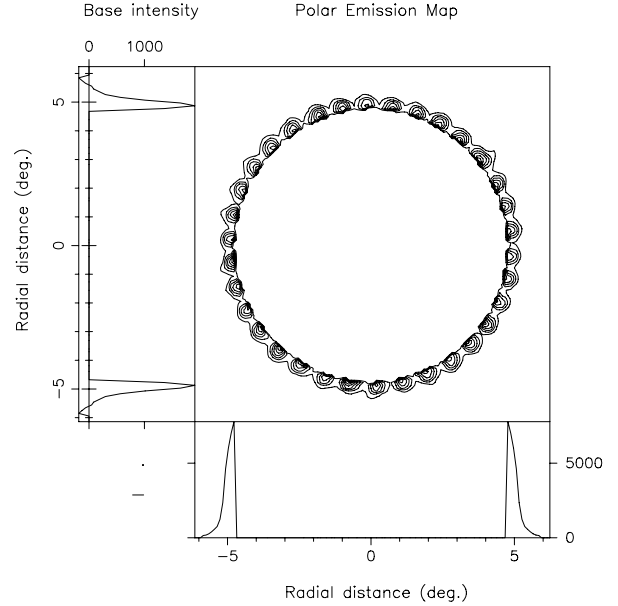


**Fig. 3.** A total-power 34-beam polar cap “map” of the accessible emission region reconstructed using the cartographic transform described in DR01. The image corresponds to the poleward or negative- $\beta$  solution in Paper I and maps the same bright 512-pulse section of the 328-MHz WSRT observation first studied in Fig. 1 (here beginning at pulse 135 so as to represent a single “carousel”-subbeam system rotation). The “drifting”-subpulse pattern is projected onto the magnetic polar cap shown in the main panel and its rotation frozen, with the “closer” rotational axis at the top of the diagram and the sightline cutting the emission pattern near “12 o’clock”. The bottom and side panels show the average- and incoherent (non-accurately drifting) “base”-intensity profiles, respectively, as functions of the angular distance from the magnetic axis. The base intensity here has not been removed from the pattern in the central panel.

total intensity. The linear power is again represented by the rotated Stokes parameter  $Q'$  which we had encountered previously in RRS. All of the significant linear power is rotated into  $Q'$ , such that one polarization mode is represented by positive values and the other by negative.

Composite subbeam maps in total and linear power are then given in Fig. 4 (top), where Stokes  $I$  is depicted as contours and the linear power  $Q'$  is color-intensity coded according to the bars on the left of the figures. In the lefthand figure the total intensity is shown fully, whereas in the righthand one the non-drifting “base” (left panels) has been subtracted so that more detail is evident. Note in the left diagram that each beamlet emits both polarization modes in a complex but systematic manner: the positive mode is strongly associated with the total power beamlets, whereas the negative mode is often strongest between the total power beamlets and tails off clockwise around the periphery of the following beamlet. Remarkably, the positive linear mode occurs almost entirely in the inner part of the conal beam near the sightline cutoff, whereas the negative mode is found over a substantial radial range. It should be added that the canted linear structures in the maps are well explored here – especially in the inner part of the pattern – as data from some 11 successive pulses contributes to the image of each such beamlet.

The very pronounced asymmetry of the subbeam linear polarization in Fig. 4 is arresting, and we must recall that this property is closely related to the “absorption”-induced asymmetry of the overall PS and its polarized profile discussed throughout RRS, Paper I and above. The top righthand display of Fig. 4 gives the total power with the non-drifting base (left panel)

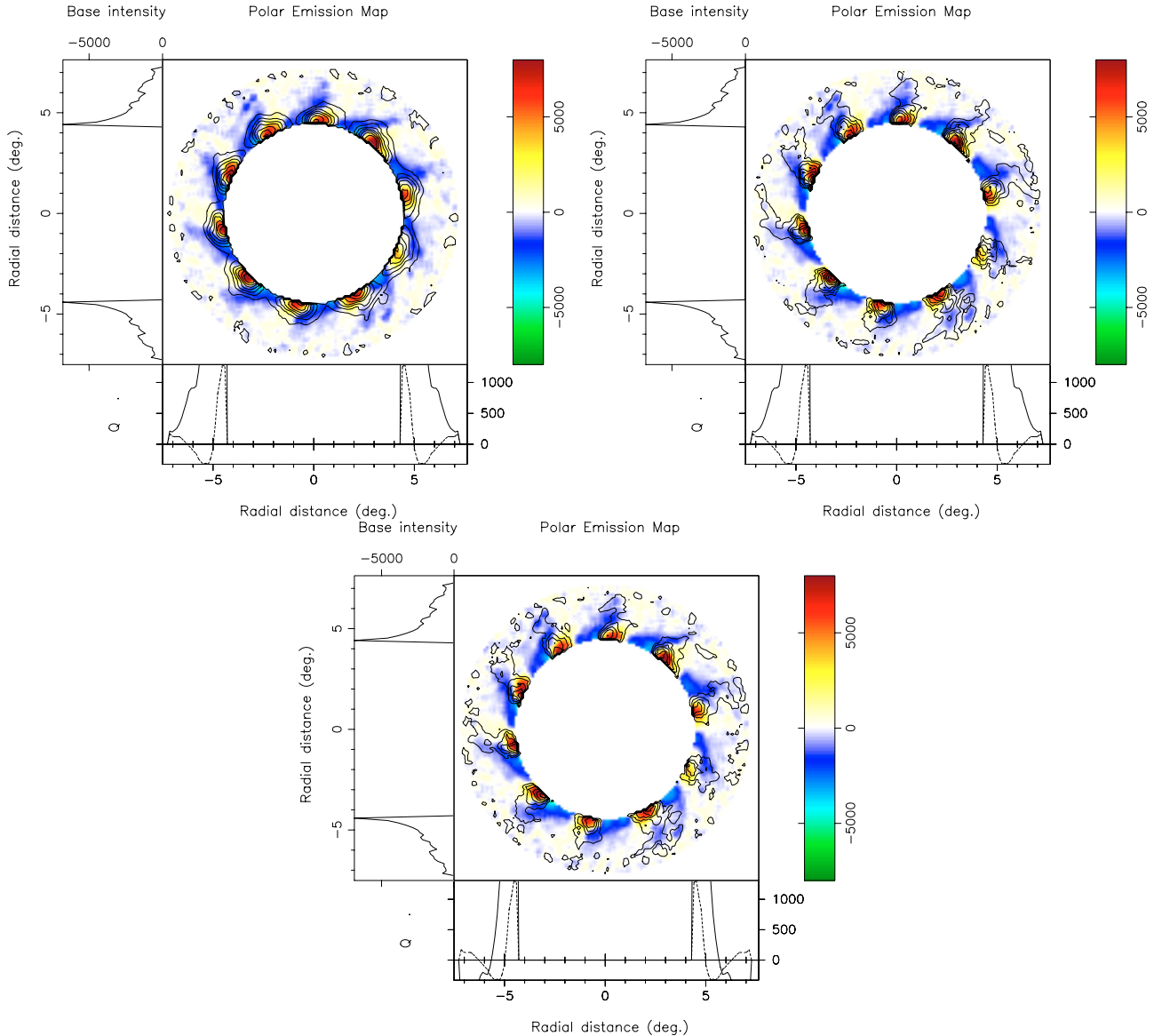


**Fig. 4.** (Top) Composite 10-subbeam maps in total power and total-linear power (Stokes  $Q'$ ) of the same 328-MHz PS as in Figs. 1–3, here corresponding to the equatorward or positive- $\beta$  sightline solution in Paper I. The contours show the total power beam-system intensities (left) as well as with the circularly symmetric “base” function (left panels) subtracted (righthand figure). The color-intensity coding gives the respective linear polarization according to the scale at the right of the diagrams. The net polarization-modal power (PPM/SPM) is here distinguished only by the sign of  $Q'$ : the positive (yellow-orange) modal “beamlets” are more intense and fall on the inside of the diagram; whereas the negative (blue-cyan-green) beamlets occur further from the magnetic axis, fall off in a canted manner and are generally weaker. Here the sightline cuts the emission pattern from right to left at the bottom of the diagrams. The total power (solid curve) and residual linear (dotted) conal beam forms are shown in the bottom panels; the total power is truncated from a maximum value of about  $2.2 \times 10^4$  arbitrary units, whereas the linear shows the different radial dependences of the two polarization modes. Here, we have used pulses 179 to 512, corresponding to three putative circulation times for the 10-beam “carousel” system. (Below) Composite unpolarized (Stokes  $I - \sqrt{Q^2 + U^2 + V^2}$ ) power (contours) and  $Q'$  (color scale) subbeam map. Here the “base” has been subtracted, and the total power beamform (bottom panel) truncated from a maximum value of about  $10^4$ .

subtracted, and here we see somewhat more detail in the individual beamlets. Clearly, the total intensity base here is comprised largely of positive- $Q'$  within the 10 beamlets and negative- $Q'$  contributions between them. In addition we see some tendency for the total power to tail off in a manner similar to that of the negative linear mode to large angular distances on the beam edge.

Finally, we note that the fractional linear polarization of subpulses within the 328-MHz PS is typically 50%, and it is interesting to ask where the beam depolarization occurs. Thus, in Fig. 4 (bottom) we have plotted the subbeam configuration in residual unpolarized power (contours) and linear power (colors)

– where the base (left panel) has been removed. If the depolarization is occurring through an incoherent superposition of polarized power near the beamlet edges, then we might expect the unpolarized power to show features near the modal beamlet boundaries. However, this is not what the map appears to show. Most of the unpolarized power is here associated with the positive- $Q'$  polarization mode – which is in turn associated with the total power beamlets in Fig. 4 (top).

Thus it would appear that the modal power in B0809+74 is angularly disjoint, and we apparently see modal depolarization only on the edges of the various modal beamlets – and it appears to be such a minor effect that it cannot really be discerned in

these several polarized subbeam maps. Indeed, one need not depend on maps such as these to draw this conclusion: simpler PS displays such as that in Ramachandran et al.'s (2002) Fig. 4 depict modal polarization boundaries in nearly every pulse, about which little mode mixing appears to occur. This said, it is tempting to entertain the conclusion that the two polarization modes are only partially polarized in B0809+74 at 328 MHz. And, even if, however, this is the case, the conclusion must stand in strong contrast to the situation at 21 cms, where we have noted (Paper I) the nearly complete linear polarization on the leading edge of the star's profile there.

The dynamic interaction of the rotating subbeam “carousel” system in the foregoing figures with the sightline to the Earth exemplifies the kind of conal beam properties which almost certainly must be encountered in most pulsars – that is, sets of modal beamlets which are offset from each other both in magnetic azimuth and polar angle. Such a conclusion was reached independently via an analysis of polarized conal single and double profiles (Rankin & Ramachandran 2003). Moreover, we can now begin to see how it is that such an interaction can produce complex and counter-intuitive behaviors such as the total power  $P_2$  variations discussed in RRS.

## 5. Discussion

We have attempted in this paper to further understand the spectacular subpulse modulation of pulsar B0809+74. Our analyses are based on high quality PSs from which the null intervals have been removed, as indicated by the techniques developed by van Leeuwen et al. (2002). The null effects cannot be completely removed, however, both because of higher-order effects and because some number of nulls, less than one  $P_1$  in duration, will occur when the star beams in other directions.

We then find that the star exhibits very little fluctuation-spectral information bearing on its “carousel” subbeam configuration. Extensive searches have been carried out using the inverse-cartographic algorithm in an effort to define its subbeam-system properties and, unfortunately, for B0809+74 these have provided no more detailed information than already could be inferred from the geometric models of Paper I. We are thus not able to decide whether the star's sightline passes poleward or equatorward of its magnetic axis, and values of the magnetic latitude  $\alpha$  and sightline impact angle  $\beta$  for the two alternative configurations are given in Paper I, Table 3.

All of our searches and correlations reiterate the conclusions of van Leeuwen et al. (2003) to the end that the star's basic subpulse modulation frequency is the true one and thus not aliased. On this basis we then find that if the star has an “inside” (poleward) sightline traverse, it could have a subbeam “carousel” system with some 25–40 beamlets, or, if an “outside” (equatorward) traverse, some 8–12. The geometric models of Paper I seem to restrict this range somewhat more, and for working purposes we have used  $N$  values of 34 and 10, respectively. Polar maps corresponding to both possibilities are given above, and physical considerations may favor the latter one, simply because of space constraints on the polar cap.

Nonetheless, either configuration implies subbeam circulation times  $\hat{P}_3$  much longer than the  $2.5 P_1$  predicted by the Ruderman & Sutherland (1975) theory. Without aliasing,  $\hat{P}_3$  is simply the product of the subbeam number  $N$  and  $P_3 = 11P_1$ , so that for an inner traverse  $\hat{P}_3$  is 280–450  $P_1$  and for an outer traverse 90–130  $P_1$ .  $\mathbf{E} \times \mathbf{B}$  drift may still be responsible for the “carousel” rotation, but in a different configuration than the polar cap “gap” region envisioned in the above theory.

Polarized polar maps have been constructed which appear to give new insight into the polarization-modal structure of the “carousel”-beam system. While our results show a complex yet systematic structure, we find as expected that the modal beamlet systems are offset from each other both in magnetic azimuth and polar angle (Rankin & Ramachandran 2003). The stronger (here positive) system is largely confined to the inner periphery of the map near the sightline limit, and the second weaker system, while also most intense on the inner periphery, tails off in an asymmetric diagonal manner over a much larger range of magnetic polar angle. The detailed modal structure of this polarized “carousel” system is well defined by the cartographic mapping. The contrasting forms of the two modal systems is unexpected and potentially important. And with such maps in mind it can hardly be surprising that their periodic encounter with our sightline could give rise to the perplexing  $P_2$  effects considered in RRS.

*Acknowledgements.* We thank Ben Stappers and Russell Edwards for interesting and useful discussions and their assistance with some of the Westerbork observations. Portions of this work were carried out with support from The Netherlands Organisatie voor Wetenschappelijk Onderzoek and US National Science Foundation Grants AST 99-87654 and 00-98685. This work made use of the NASA ADS astronomical data system.

## References

- Backer, D. C. 1970a, *Nature*, 227, 692
- Backer, D. C. 1970b, *Nature*, 228, 42
- Backer, D. C. 1970c, *Nature*, 228, 752
- Backer, D. C. 1970d, *Nature*, 228, 1297
- Backer, D. C. 1971, Ph.D. Thesis, Cornell Univ.
- Backer, D. C. 1973, *ApJ*, 182, 245
- Backer, D. C., & Rankin, J. M. 1980, *ApJS*, 42, 143
- Backer, D. C., Rankin, J. M., & Campbell, D. B. 1975, *ApJ*, 197, 481
- Cole, T. W. 1970, *Nature*, 227, 788
- Deshpande, A. A., & Rankin, J. M. 1999, *ApJ*, 524, 1008
- Deshpande, A. A., & Rankin, J. M. 2001, *MNRAS*, 322, 438
- Drake, F. D., & Craft, H. D. Jr 1968, *Nature*, 220, 231
- Edwards, R. T., & Stappers, B. W. 2003, *A&A*, 410, 961
- Edwards, R. T., & Stappers, B. W. 2004, *A&A*, 421, 681
- Filippenko, A. V., & Radhakrishnan, V. 1982, *ApJ*, 263, 828
- Filippenko, A. V., Readhead, A. C. S., & Ewing, M. S. 1983, in *Positron-Electron Pairs in Astrophysics*, AIP Conf. Proc., 101, 113
- van Leeuwen, A. G. J., Kouwenhoven, M. L. A., Ramachandran, R., Rankin, J. M., & Stappers, B. W. 2002, *A&A*, 387, 169
- van Leeuwen, A. G. J., Stappers, B. W., Rankin, J. M., & Ramachandran, R. 2003, *A&A*, 399, 223
- Lyne, A. G., & Ashworth, M. 1983, *MNRAS*, 204, 477
- Lyne, A. G., & Manchester, R. N. 1988, *MNRAS*, 234, 519
- Lyne, A. G., Smith, F. G., & Graham, D. A. 1971, *MNRAS*, 153, 337
- Manchester, R. N., Taylor, J. H., & Huguenin, G. R. 1975, *ApJ*, 196, 83
- Page, C. G. 1973, *MNRAS*, 163, 29
- Popov, M. V., & Smirnova, T. V. 1982, *Sov. Astron.*, 26, 439
- Ramachandran, R., Rankin, J. M., Stappers, B. W., Kouwenhoven, M. L. A., & van Leeuwen, A. G. L. 2002, *A&A*, 381, 993
- Rankin, J. M. 1993a, *ApJ*, 405, 285 (EP Paper VIa)
- Rankin, J. M. 1993b, *ApJS*, 85, 145 (EP Paper VIb)
- Rankin, J. M., & Ramachandran, R. 2003, *ApJ*, 590, 411
- Rankin, J. M., Ramachandran, R., & Suleymanova, S. A. 2005, *A&A*, 429, 999 (RRS)
- Rankin, J. M., Ramachandran, R., & Suleymanova, S. A. 2006, *A&A*, 447, 235 (Paper I)
- Ruderman, M. A. 1972, *ARA&A*, 10, 427
- Ruderman, M. A. 1976, *ApJ*, 203, 206
- Ruderman, M. A., & Sutherland, P. G. 1975, *ApJ*, 196, 51
- Sutton, J. M., Staelin, D. H., Price, R. M., & Weimer, R., 1970, *ApJ*, 159, L89
- Taylor, J. H., & Huguenin, G. R. 1971, *ApJ*, 167, 273
- Taylor, J. H., Huguenin, G. R., Hirsch, R. M., Manchester, R. M. 1971, *ApLett*, 9, 205
- Taylor, J. H., Jura, M., & Huguenin, G. R. 1969, *Nature*, 223, 797
- Unwin, S. C., Readhead, A. C. S., Wilkinson, P. N., & Ewing, M. S. 1978, *MNRAS*, 182, 711
- Vitkevich, V. V., & Shitov, Yu. P. 1970, *Nature*, 225, 248